Int. J. Heat Mass Transfer. Vol. 32, No. 9, pp. 1605–1618, 1989
Printed in Great Britain

0017–9310/89 $3.00 + 0.00

Droplet vaporization model for spray combustion calculations

B. ABRAMZON and W. A. SIRIGNANO
Department of Mechanical Engineering, University of California, Irvine, CA 92717, U.S.A.

(*Received* 18 *May* 1988 *and in final form* 13 *December* 1988)

Abstract—The re-examination of the classical droplet vaporization model is made in order to develop the simple but sufficiently accurate calculation algorithm which can be used in spray combustion calculations. The new model includes the effects of variable thermophysical properties, non-unitary Lewis number in the gas film, the effect of the Stefan flow on heat and mass transfer between the droplet and the gas, and the effect of internal circulation and transient liquid heating. To evaluate the competing simplified models of the droplet heating, the more-refined, extended model of heat transfer within a moving circulating droplet is considered. A simplified, one-dimensional 'effective conductivity' model is formulated for the transient liquid heating with internal circulation. As an illustration, the dynamic and vaporization histories of the droplets injected into the steady and fluctuating hot air streams are analyzed.

INTRODUCTION

THE THEORETICAL analyses of spray combustion in liquid-fueled engines often use the deterministic approach [1] which requires the simultaneous calculations of trajectories and vaporization rates of many individual droplets. These droplets are injected into the combustion chamber at different times, and have various initial sizes and velocities. The prediction of such important characteristics as the geometry of the spray or an ignition position depends significantly on the model selected for the single droplet vaporization/combustion analysis.

The theory of fuel droplet vaporization/combustion has been intensively developed during the past several decades. Detailed discussions of state-of-the-art on the subject until 1986 may be found in the reviews by Sirignano [1–4], Faeth [5], Law [6] and Williams [7]. The classical droplet vaporization model is described in many textbooks on combustion (see, e.g. Kuo [8] and Williams [9]). This model is based on many oversimplified assumptions, such as a unit Lewis number in the gas phase near the droplet. To account for the effect of forced convection in the gas phase, the vaporization rate of the droplet in a stagnant environment is simply multiplied by an empirical correction factor $0.5Nu_0$, where $Nu_0 = Nu_0(Re, Pr)$ is the Nusselt number for a solid non-vaporizing sphere. Variations in physical properties are neglected; average properties and unitary Lewis number are employed. The effect of the Stefan flow (blowing) on heat and mass transfer between the moving droplet and the gas flow is assumed to be the same as in the case of the stagnant droplet. The droplet surface is postulated to be at the normal boiling temperature, and transient liquid heating is neglected. In reality, however, the Lewis number may vary considerably (in the range of 1–4) during the vaporization period; the Stefan flow effect may depend on the droplet Reynolds number; and the transient liquid heating appears to be a controlling factor of the droplet vaporization rate [1].

The importance of the process of transient liquid heating has been demonstrated in ref. [10] for the case of a stagnant vaporizing droplet ($Re = 0$). In typical combustion situations, the duration of the transient droplet heating is comparable with the droplet vaporization time. Therefore, the adequate description of the heat transfer inside the droplet is the important part of the vaporization model. References [25, 26] found that the liquid circulation inside the moving droplet may considerably change the time scale of the internal heating process. Several approximate models have been suggested in the literature to describe the different regimes of heat transfer inside the droplets. More detailed discussion of these models will be given in the next section.

Recently, the comprehensive computational studies of the dynamics of a single vaporizing droplet inserted into a hot gas flow have been undertaken by several authors [11–16]. Renksizbulut and Yuen [11] presented the finite-difference analysis of flow and heat and mass transfer around the vaporizing heptane sphere including the effects of blowing and variable physical properties. However, the specific heat of fuel vapor and air were treated as equal and constant. Unfortunately, the latter assumption is invalid for the hydrocarbon fuels where, for example, the ratio $C_{pF}/C_{air} \simeq 3$ at $T = 600°C$. Patnaik *et al.* [12] and Dwyer and Sanders [13, 14] analyzed the dynamics of the evaporating droplet including the effects of transient convection, Stefan flow, internal circulation and liquid heating. The viscosity of the fuel vapor/air mixture was variable and other thermophysical properties were calculated assuming the constant values of the Schmidt and Prandtl numbers: $Sc = 2$, $Pr = 0.7$. Haywood and Renksizbulut [15, 16] presented the finite-difference calculations of the life his-

NOMENCLATURE

A_r	averaging parameter
B_M	mass transfer number
B_T	heat transfer number
C_D	droplet drag coefficient
C_F	friction drag coefficient
C_{pF}	fuel vapor specific heat
D	vapor/air binary diffusion coefficient
F	relative change of film thickness
j	iteration number
k	thermal conductivity
Le	Lewis number, $k_g/(\rho_g D C_{pg})$
$\dot{m}$	vaporization rate [g s^{-1}]
m_0	initial droplet mass [g]
Nu	Nusselt number
P	pressure
Pe	Peclet number, $Re\,Pr$
Pr	Prandtl number
Q_L	heat transferred into the droplet [cal s^{-1}]
r	radius [cm]
r_0	initial droplet radius
r_s	instantaneous droplet radius; $r_s' = r_s/r_0$
Re	Reynolds number
Sc	Schmidt number
Sh	Sherwood number
T	temperature [K]
t	time
U	droplet velocity
U_s	maximum velocity on the droplet surface
U_∞	gas flow velocity
V_r, V_θ	radial and angular components of liquid velocity
W_i	molecular weight of ith component
X	distance travelled by the droplet
x	molar fraction
Y	mass fraction.

Greek symbols

α	thermal diffusivity
δ	film thickness
μ	dynamic viscosity
ρ	density
ϕ	non-dimensional parameter defined by equation (22)
χ	effective conductivity parameter.

Subscripts

air	air
f	film
F	fuel vapor
g	gas
L	liquid
M	mass diffusion problem
s	surface
T	thermal problem
∞	far from a droplet
0	initial state (also without the Stefan flow).

Superscripts and overscore

$\bar{}$	average (reference) value
*	modified value
′	non-dimensional value.

tory of an n-heptane droplet moving and evaporating in its own super-heating vapor. Both the effects of variable properties and internal circulation and heating were taken into consideration. It is unclear, however, if their results are applicable to the practical case of a non-vapor environment where the diffusion may be one of the controlling factors in the vaporization process.

It should be noted that the studies [12–16] lead to some partially conflicting conclusions about the droplet drag coefficient, C_D. Dwyer and Sanders [13, 14] found that C_D decreases significantly as the droplet vaporizes and the relative velocity between the droplet and gas decreases. In contrast, Haywood and Renksizbulut [15, 16] observed that the drag coefficient increases in the course of droplet motion and vaporization, and the 'standard drag curve', $C_D = C_D(Re)$, of a solid sphere may be used for a vaporizing droplet provided the thermophysical properties in the gas film are evaluated at some average temperature and the appropriate correction is made to account for the blowing effect. Note, however, all investigators are making calculations in different parameter regimes. The above discussion shows that additional efforts are required in order to obtain a better understanding of the droplet dynamics and the vaporization/combustion process.

It is emphasized that the advanced numerical models cannot be directly adopted for the spray combustion calculations, primarily due to the great amount of computer time needed for a single droplet analysis. (However, the exact numerical solutions may be very useful for improvement of the approximate models currently used in spray combustion calculations.) In the present study, we have formulated a new approximate droplet vaporization model which can be suitable for the spray combustion calculations. In spite of its simplified character, the new model accounts for many important physical effects mentioned above.

THEORY

Droplet dynamics

For simplicity, we consider a case where the gas flow is one-dimensional and the initial droplet velocity is parallel to the gas flow direction. The droplet motion and radius reduction are governed by the following equations:

$$\frac{dX}{dt} = U \tag{1}$$

$$\frac{dU}{dt} = \frac{3C_D}{2r_s}\left(\frac{\rho_\infty}{\rho_L}\right)|U_\infty - U|(U_\infty - U) \tag{2}$$

$$\frac{dr_s}{dt} = -\frac{\dot{m}}{4\pi\rho_L r_s^2}. \tag{3}$$

The drag coefficient is usually expressed as a function of the Reynolds number, $C_D = C_D(Re)$, where $Re = 2\rho_\infty|U_\infty - U|r_s/\overline{\mu_g}$. Since the Reynolds number is interpreted as a ratio of inertia to viscous forces, the definition of Re uses the free-stream density, ρ_∞, and some average viscosity, $\overline{\mu_g}$, of the air/vapor mixture in the boundary layer near the droplet surface. As experimentally shown by Yuen and Chen [17], the drag coefficient of evaporating droplets may be well approximated by the 'standard drag curve' provided the gas viscosity, $\overline{\mu_g}$, is evaluated at some reference temperature and fuel concentration

$$\bar{T} = T_s + A_r(T_\infty - T_s);\ \bar{Y}_F = Y_{Fs} + A_r(Y_{F\infty} - Y_{Fs}) \tag{4}$$

where A_r is the averaging parameter. Yuen and Chen [17] recommended the value $A_r = 1/3$ ('1/3 rule'). However, the experiments in ref. [17] were conducted at relatively low gas temperatures with the transfer number $B = \bar{C}_p(T_\infty - T_s)/L \leqslant 3$. Additional research is required to determine properly the values of C_D for larger vaporization rates.

In the present study we used the above recommendation [17] along with the following correlation for the 'standard drag curve' [5]:

$$C_D = \frac{24}{Re}\left[1 + \frac{Re^{2/3}}{6}\right]. \tag{5}$$

For dense spray regions, where the distance between droplets is comparable with the droplet's diameter, the drag coefficient should also depend on the local droplet concentration in the gas flow. As new correlations including these effects become available, they can replace equation (5) in the present droplet vaporization model. Note that Haywood and Renksizbulut [15, 16] has recommended a mass transfer correction to equation (5).

Gas-phase analysis

The analysis of heat and mass transfer processes in the gas phase near the droplet surface allows the determination of the instantaneous vaporization rate, $\dot{m}$, and the amount of heat penetrating into the droplet interior, Q_L. In this study we use the gas-phase model which has been recently developed by the present authors [18]. Below is a discussion of the general assumptions of the model and the final computational algorithm.

We assume that the gas phase heat and mass transfer may be considered as quasi-steady, the pressure drop in the gas is negligible, and the thermophysical properties may be treated as a constant provided they are evaluated at some reference conditions (see equation (4)). These assumptions supported, in particular, by the results of Hubbard *et al.*'s [19] study that analyzed the stagnant droplet ($Re = 0$) vaporization at $P \leqslant 10$ atm including transients and variable properties effects. They also recommended the use of the '1/3 rule' ($A_r = 1/3$) for the thermophysical properties averaging procedure. Note that as Reynolds number increases, the quasi-steady assumption becomes even more justified since the relaxation time for the transport processes in the gas boundary layer decreases as $t_{relax} \sim r/\Delta U_\infty = r^2/(\nu_g Re)$, while the droplet vaporization time varies approximately as $1/Re^{0.5}$ at high Re.

To take into account the effect of the convective transport caused by the droplet motion relative to the gas, we employ the so-called 'film theory' [20, 21]. The film theory assumes that the resistance to heat or mass exchange between a surface and a gas flow may be modelled by introducing the concept of gas films of constant thicknesses: δ_T, δ_M. Thus, for the non-vaporizing spherical particle, the thicknesses of the thermal and diffusional films are calculated as

$$\delta_{T0} = \frac{2r_s}{Nu_0 - 2};\ \delta_{M0} = \frac{2r_s}{Sh_0 - 2} \tag{6}$$

where $Nu_0 = Nu_0(Re, Pr)$ and $Sh_0 = Sh_0(Re, Sc)$ are the Nusselt and Sherwood numbers, respectively. Expressions (6) are derived from the requirement that the rates of a purely molecular transport by thermal conduction or diffusion through the film must be equal to the actual intensity of the convective heat or mass transfer between the surface and the external flow. The classical film model uses the same expressions (6) for an evaporating droplet. However, the presence of the Stefan flow will influence the values of δ_T and δ_M, since a surface blowing results in the thickening of the laminar boundary layer [22]. To take into consideration this effect, we introduce the correction factors

$$F_T = \delta_T/\delta_{T0};\ F_M = \delta_M/\delta_{M0} \tag{7}$$

which represent the relative change of the film thicknesses due to the Stefan flow. The expressions for F_T and F_M will be considered below.

As in other approximate models, the film model assumes that the distribution of the temperature and fuel vapor concentrations along the droplet surface are uniform. This assumption may cause some under-

estimation of the droplet vaporization rate since the nonlinearity of the relationship between the local surface temperature and fuel vapor pressure (Clausius–Clapeyron equation) does not justify the usage of the same relation for the surface-averaged values.

Finally, the extended film model yields the following expressions for the instantaneous droplet vaporization rate:

$$\dot{m} = 2\pi\bar{\rho}_g\bar{D}_g r_s Sh^* \ln(1+B_M) \tag{8}$$

and

$$\dot{m} = 2\pi\frac{\bar{k}_g}{\bar{C}_{pF}} r_s Nu^* \ln(1+B_T) \tag{9}$$

where $\bar{\rho}_g$, $\bar{D}_g$, and $\bar{k}_g$ are the average density, binary diffusion coefficient and thermal conductivity of the gas mixture in the film, respectively; $\bar{C}_{pF}$ is the average vapor specific heat in the film; Sh^* and Nu^* are the non-dimensional parameters which are expressed as

$$Sh^* = 2+(Sh_0-2)/F_M \tag{10}$$

$$Nu^* = 2+(Nu_0-2)/F_T. \tag{11}$$

The values B_M and B_T are called the Spalding mass and heat transfer numbers, and they are calculated as

$$B_M = \frac{Y_{Fs}-Y_{F\infty}}{1-Y_{Fs}} \tag{12}$$

$$B_T = \frac{\bar{C}_{pF}(T_\infty - T_s)}{L(T_s)+Q_L/\dot{m}}. \tag{13}$$

Here Y_F is the fuel mass fraction, $L(T_s)$ the latent heat of vaporization at temperature T_s; subscripts s and ∞ refer to the conditions at the droplet surface and external gas flow, respectively.

Equations (8) and (9) resemble very closely the corresponding expressions for the droplet vaporization rate predicted by the classical model. The only difference is that the values of Nu_0 and Sh_0 in the classical formulas are substituted by Nu^* amd Sh^*, respectively. Note also that $Nu^* \to Nu_0$ and $Sh^* \to Sh_0$ as $F_T \to 1$ and $F_M \to 1$. For these reasons, the parameters Nu^* and Sh^* may be termed as 'modified' Nusselt and Sherwood numbers. Note, however, that these parameters should not be confused with the actual Nusselt and Sherwood numbers which are defined as non-dimensional heat and mass transfer coefficients

$$Nu = -\frac{2r_s}{(T_s-T_\infty)}\left(\frac{dT}{dr}\right)_s;$$

$$Sh = -\frac{2r_s}{(Y_{Fs}-Y_{F\infty})}\left(\frac{dY_F}{dr}\right)_s. \tag{14}$$

Thus, for example, the actual Sherwood number is expressed in the present model as

$$Sh = Sh^*\frac{\ln(1+B_M)}{B_M}. \tag{15}$$

To find the correction factors F_M and F_T for the film thickness, we considered a model problem of the laminar boundary layer flow past a vaporizing wedge. The range of parameters was: $0 \leqslant (B_T, B_M) \leqslant 20$; $1 \leqslant (Sc, Pr) \leqslant 3$; $0 \leqslant \beta \leqslant 2\pi$ (here β is the wedge angle). In the case of an isothermal surface and constant physical properties of the fluid, the problem has a self-similar solution and the correction factors F_M and F_T do not depend on the local Reynolds number. It was found that the values F_M and F_T are practically insensitive to the Schmidt and Prandtl numbers and the wedge angle variations, and can be approximated as

$$F_M = F(B_M),\ F_T = F(B_T) \tag{16}$$

where $F(B)$ is the universal function

$$F(B) = (1+B)^{0.7}\frac{\ln(1+B)}{B}. \tag{17}$$

Note that $F(B)$ increases from 1 to 1.285 as B grows from 0 to 8. In the interval $8 \leqslant B \leqslant 20$, the values of $F(B)$ remain practically constant.

We assume that equations (16) and (17) may also be used for the case of the evaporating droplet. At high Reynolds numbers, when $Nu_0 \gg 2$, equations (8), (10), and (17) predict that the vaporization rate varies as $\dot{m} \sim B_T(1+B_T)^{-0.7}$. The latter result is in qualitative agreement with the experimental data of Renksizbulut and Yuen [23] for water, methanol and heptane droplets in the range of $25 < Re < 2000$ and $B_T < 2.8$.

Consider now the practical step-by-step procedure of determination of the vaporization rate $\dot{m}$ and the heat transferred into the droplet interior, Q_L. Assume that we know the droplet surface temperature T_s, velocity U, and the conditions of the free-stream flow: U_∞, T_∞, $Y_{F\infty}$. The solution algorithm is given below.

(1) Calculate the molar and mass fuel vapor fractions at the droplet surface

$$x_{Fs} = P_{Fs}/P,\ Y_{Fs} = x_{Fs}W_F/\sum_i x_i W_i. \tag{18}$$

Here P_{Fs} is the fuel vapor saturated pressure which is evaluated using the appropriate experimental or theoretical correlations (Clasius–Clapeyron)

$$P_{Fs} = P_{Fs}(T_s). \tag{19}$$

(2) Calculate the average physical properties

$$\bar{\rho}, \bar{C}_{pF}, \bar{C}_{pg}, \bar{k}_g, \bar{\mu}_g, \bar{D}, \overline{Le} = \bar{k}_g/(\bar{\rho}_g\bar{D}\bar{C}_{pg}), \overline{Pr}, \overline{Sc}$$

in the gas film using the reference conditions given by equation (4).

(3) Calculate the Reynolds number, $Re = 2\rho_\infty|U-U_\infty|r_s/\mu_g$, and the Nusselt and Sherwood number for a non-vaporizing droplet. The well-known Frossling correlations may be used for Nu_0 and Sh_0 evaluations

$$Nu_0 = 2+0.552Re^{1/2}Pr^{1/3};$$

$$Sh_0 = 2+0.552Re^{1/2}Sc^{1/3}. \tag{20}$$

Note that equations (20) overestimate the transfer

rate at low Reynolds numbers ($Re \leqslant 10$). Particularly, they predict the physically incorrect supersensitivity of the transfer rate to the small velocity fluctuations near $Re = 0$, since $(\partial Nu_0/\partial Re)_{Re=0} = \infty$. As noted by Crocco [43], this fact may result in erroneous conclusions during a combustion instability analysis.

As an alternative to equations (20), the following correlations by Clift *et al.* [24] may be recommended:

$$Nu_0 = 1 + (1 + Re\,Pr)^{1/3} f(Re)$$

$$Sh_0 = 1 + (1 + Re\,Sc)^{1/3} f(Re) \qquad (21)$$

where $f(Re) = 1$ at $Re \leqslant 1$ and $f(Re) = Re^{0.077}$ at $Re \leqslant 400$. Equations (21) approximate the numerical results by different authors in the range of $0.25 < (Pr, Sc) < 100$ with an error less than 3%.

(4) Calculate the Spalding mass transfer number, B_M, diffusional film correction factor, F_M, modified Sherwood number, Sh^*, and the mass vaporization rate, $\dot{m}$ (equations (12), (17), (10) and (8)).

(5) Calculate the correction factor for the thermal film thickness, $F_T = F(B_T)$, using the value of the heat transfer number, B_T^{old}, from the previous iteration or previous time step (equation (17)).

(6) Calculate the modified Nusselt number, Nu^* (equation (11)), the parameter

$$\phi = \left(\frac{\bar{C}_{pF}}{\bar{C}_{pg}}\right)\left(\frac{Sh^*}{Nu^*}\right)\frac{1}{Le} \qquad (22)$$

and the corrected value of the heat transfer number

$$B_T = (1 + B_M)^{\phi} - 1. \qquad (23)$$

Return to step (5) if $|B_T - B_T^{old}| < \varepsilon_B$, where ε_B is the desired accuracy of the B-number evaluation.

(7) Calculate the heat penetrating into the liquid phase

$$Q_L = \dot{m}\left\{\frac{\bar{C}_{pF}(T_\infty - T_s)}{B_T} - L(T_s)\right\}. \qquad (24)$$

Liquid phase analysis

A knowledge of the instantaneous heat transferred into the liquid phase (equation (24)) allows us to predict the temperature inside the droplet as a function of time. The transient droplet temperature is often calculated using the following simplified models [1, 6]:

(a) the 'rapid mixing limit' or 'infinite conductivity model' which postulates that the temperature within the droplet is spatially uniform although time varying;

(b) the 'conduction limit' model which assumes that the heat is transferred within the liquid solely by the thermal conduction and the surface temperature is uniform.

These models are usually considered as two extremes bounding the possible range of real conditions. References [25, 26] demonstrated that heat transfer within moving droplets is of the pronounced convective type due to the intensive liquid circulation caused by the surface friction. The Reynolds and Peclet numbers for the droplet interior, which can be defined as

$$Re_L = \frac{U_s d \rho_L}{\mu_L}\,;\; Pe_L = Re_L\,Pr_L \qquad (25)$$

appear to be very large compared to unity. In equations (25), U_s is the maximum velocity at the droplet surface (in the coordinate system related to the droplet), and subscript 'L' refers to the liquid phase. References [27–29] developed the 'vortex model' which assumes that the internal circulation in the droplet is represented by the well-known Hill vortex and, due to the high liquid Peclet number, Pe_L, the isotherms inside the droplet coincide with the streamlines.

Comparisons between different simplified models in spray calculations were made by Aggarwal *et al.* [30]. It was found that the instantaneous droplet radius as a function of time predicted by the vortex model falls between those given by the rapid mixing and conduction limit models.

The instantaneous vaporization rate is extremely sensitive to the selection of the liquid heating model. To compare amongst different simplified models, we undertake first a more detailed analysis of the heat transfer inside the moving droplet. The general assumptions of the extended model are given below.

(a) Temperature distribution along the droplet surface is uniform but time varying.

(b) Instantaneous velocity field inside the moving evaporating droplet may be approximated by the Hill spherical vortex solution

$$V_r = U_s(1 - r^2/r_s^2)\cos\theta \qquad (26)$$

$$V_\theta = U_s(1 - 2r^2/r_s^2)\sin\theta \qquad (27)$$

where V_r' and V_θ' are the radial and angular components of liquid velocity in the spherical coordinate system (r, θ). The maximum surface velocity varies as a function of time.

The first assumption is made in order to be consistent with the one-dimensional gas-phase model which operates with the average surface temperature and cannot predict the local distribution of the surface temperature or heat flux. The second assumption is based on the numerical results of Rivkind and Ryskin [34], Oliver and Chung [35], and other authors (see, ref. [24]) who analyzed the flow structures inside and outside the droplet moving at terminal velocity in another viscous fluid. For a wide range of conditions (Reynolds numbers, ratios of fluid viscosities and densities), their internal streamline patterns were insensitive to the internal Reynolds number and resemble very closely the Hill vortex. We assume that the same Hill vortex solution, equations (26) and (27), is also applicable to the unsteady situation when the droplet vaporizes and its velocity relative to the gas varies with time. The characteristic time of stabilization of the velocity field inside the droplet, t_{hydr}, depends on

the liquid Reynolds number. At $Re_L \leqslant 1$ (viscous regime), this time may be estimated at $t_{hydr} \sim r_s^2/\nu_L$. At high liquid Reynolds number ($Re_L \gg 1$), the vorticity disturbance is transferred from the surface into the droplet depth by convection and $t_{hydr} \sim r_s/U_s = r_s^2/(\nu_L Re_L)$. Since the Prandtl number for liquid fuel is about 10, the value of t_{hydr} appears to be much shorter than the characteristic heating time: $t_{therm} \sim r_s^2/\alpha_L$. Therefore, the use of velocity profiles (26) and (27) in the transient heating analysis is justified.

To find the maximum liquid velocity at the surface, U_s, we recall that the friction component of the droplet drag force is calculated as

$$F_{frict} = 2\pi r_s^2 \int_0^\pi (\tau_{r\theta})_g \sin^2\theta \, d\theta \tag{28}$$

where $(\tau_{r\theta})_g$ is the shear stress on the droplet surface from the gas side [20]. Since the shear stresses are continuous through the interface between the gas and liquid

$$(\tau_{r\theta})_g = (\tau_{r\theta})_L \tag{29}$$

the value of $\tau_{r\theta}$ may be evaluated using the known velocity distributions, equations (26) and (27), on the liquid side. Finally, the maximum surface velocity is expressed as

$$U_s = \frac{1}{32}\Delta U_\infty \left(\frac{\mu_g}{\mu_L}\right) Re_\infty C_F \tag{30}$$

where C_F is the friction drag coefficient, and $\Delta U_\infty = U_\infty - U$ is the relative gas/droplet velocity.

In general, C_F is a function of the Reynolds number, fluid viscosity ratio μ_L/μ_g, density ratio ρ_L/ρ_g and the transfer number B. The data on the friction drag coefficient of a moving evaporating droplet are absent in the literature. For a solid non-vaporizing sphere, the available numerical data on C_F [24] can be correlated as

$$C_F = 12.69 Re^{-2/3} \quad (10 \leqslant Re \leqslant 100). \tag{31}$$

Upon substitution into equation (30), the latter correlation produces a satisfactory prediction of the maximum surface velocity of a non-vaporizing droplet at $\mu_L/\mu_g \geqslant 10$. Thus, for example, at $Re_\infty = 100$ and viscosities ratios $\mu_L/\mu_g = 10$ and 55, equations (30) and (31) yield: $U_s/\Delta U_\infty = 0.184$ and 0.0335, respectively. The numerical solutions by Rivkind and Ryskin [34] and LeClair *et al.* [36] give for the same conditions $U_s/\Delta U_\infty = 0.2$ and 0.036, respectively.

For the case of an evaporating sphere, Renksizbulut and Yuen [11] found that the Stefan flow reduces the friction drag coefficient by a factor $(1+B)$. This results in the correlation

$$C_F = \frac{12.69}{Re^{2/3}(1+B_M)} \tag{32}$$

which has been used as a first approximation in the present model. It should be noted, however, that the computational study [11] considered only small transfer numbers ($B < 0.78$). The analysis by Emmons [37] for the boundary layer flow over the evaporating plate shows that the friction drag is reduced approximately by a factor $(1+B)^{0.75}$ at $B < 20$. Obviously, additional efforts are required to determine C_F for an evaporating droplet at high values of B.

The transient heat transfer inside the circulating and evaporating droplet is governed by the following dimensionless energy equation:

$$(r_s')^2 \frac{\partial Z}{\partial \tau} + (0.5 Pe_L V_r' r_s' - \beta\eta)\frac{\partial Z}{\partial \eta} + 0.5 Pe_L \frac{V_\theta' r_s'}{\eta}\frac{\partial Z}{\partial \theta} = \frac{1}{\eta^2}\frac{\partial}{\partial \eta}\left(\eta^2 \frac{\partial Z}{\partial \eta}\right) + \frac{1}{\eta^2 \sin\theta}\frac{\partial}{\partial \theta}\left(\sin\theta \frac{\partial Z}{\partial \theta}\right). \tag{33}$$

Here $r_s' = r_s/r_0$ is the non-dimensional radius of the droplet; $\eta = r/r_s$ is the non-dimensional radial coordinate; $V_r' = V_r/U_s$ and $V_\theta' = V_\theta/U_s$ are the non-dimensional radial and tangential velocity components; $Z = (T - T_0)/T_0$ is the non-dimensional temperature; $\tau = \alpha_L t/r_0^2$ is the non-dimensional time; $\beta = 0.5 d(r_s')^2/d\tau$ is the non-dimensional parameter proportional to the surface regression rate of the droplet. The initial and boundary conditions are given below.

(a) Uniform initial temperature

$$\tau = 0, \quad Z = 0. \tag{34}$$

(b) Uniform temperature and given total heat flux at the surface

$$\eta = 1; \quad \partial Z/\partial\theta = 0 \tag{35}$$

$$\int_0^\pi \left(\frac{\partial Z}{\partial \eta}\right)\sin\theta \, d\theta = Q_L/(2\pi r_s k_L T_0). \tag{36}$$

(c) Symmetry condition along the axis

$$\theta = 0, \pi, \quad \partial Z/\partial\theta = 0. \tag{37}$$

It is easily seen that the extended model, equations (33)–(37), includes the previous simplified models as the limiting cases. For example, at $Pe_L \to 0$ the extended model reduces to the 'conduction limit' model. In the opposite limiting case of very high Pe_L, the convective transport inside the droplet is much stronger than thermal diffusion transfer, and hence the isotherms may be expected to coincide with the streamlines ('vortex' model). The third limiting case of $k_L \to \infty$ represents the 'infinite conductivity' model.

Recently, an alternative approach has been suggested [31, 32] in order to simplify the calculation procedure for internally circulating droplets. This approach is equivalent to the conduction limit model for the use of the 'effective' value of the thermal conductivity coefficient inside the droplet: $k_{eff} = \chi k_L$ ($\chi \geqslant 1$). Such an idea was first introduced by Kronig and Brink [33] who studied mass transfer inside the

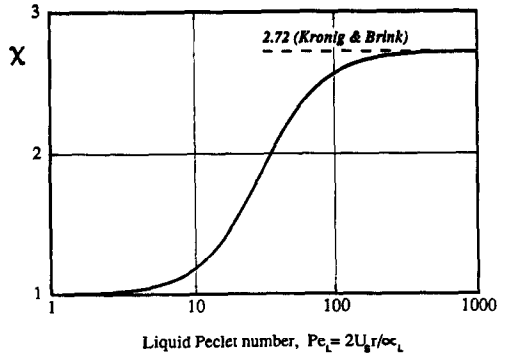

FIG. 1. Effective thermal conductivity factor vs liquid Peclet number. Approximate results of equation (39).

droplets for Hill's type of internal circulation at high Peclet numbers. They found that in the asymptotic regime ($\tau \to \infty$), the overall heat or mass transfer rate between the droplet interior and the surface is 2.72 times higher than in the case of the solid sphere. This fact may be formally interpreted as an increasing of the sphere thermal conductivity by a factor $\chi = 2.72$. Such an approach can be called the 'effective conductivity model'.

Jin and Borman [32] approximated the results by Kronig and Brink to find the coefficient χ as a function of time. Talley and Yao [31] found that using the constant factor $\chi = 2.25$ may well fit the vortex model results. Theoretically, the factor χ should also depend on the liquid Peclet number, Pe_L.

In the present study, we considered the 'effective conductivity model' where the factor $\chi = \chi(Pe_L)$ was found based on the numerical results by Johns and Beckmann [38] for mass transfer inside a circulating droplet at intermediate Pe_L. Johns and Beckmann calculated the asymptotic Nusselt number for the internal problem, $Nu_{in} = Nu_{in}(Pe_L)$. The value of Nu_{in} varies between $Nu_{in}(0) = 6.58$ for a solid sphere and $Nu_{in}(\infty) = 17.9$ for $Pe_L \to \infty$. The factor χ is calculated as

$$\chi = Nu_{in}(Pe)/Nu_{in}(0) \tag{38}$$

and varies over the range of 1–2.72. We found the following approximation which fits the Johns and Beckmann data within $\pm 2\%$:

$$\chi = 1.86 + 0.86 \tanh [2.245 \log_{10} (Pe_L/30)]. \tag{39}$$

This curve is shown in Fig. 1.

Numerical method

The ordinary differential equations (1)–(3) were solved by the implicit iterative method of second-order accuracy with respect to time [39]. The right-hand sides of equations (1)–(3) are calculated using the arithmetic mean values of variables r_s, T_s, U, X at time levels t and $(t+\Delta t)$, as for instance

$$\bar{T}_s = 0.5[T_s(t) + T_s^j(t+\Delta t)].$$

Here j is the iteration number. An initial estimation for $T_s(t+\Delta t)$ is taken to be equal to $T_s(t)$. The iterations are terminated when the following conditions are satisfied:

$$|T_s^{j+1} - T_s^j| < 0.01 \text{ K}$$

$$|(\dot{m}^{j+1} - \dot{m}^j)/\dot{m}^j| < 0.01.$$

The internal droplet temperature for the conduction limit or effective conductivity models was calculated using the Crank–Nicolson scheme. The number of grid intervals in the radial direction inside the droplet was usually 100, the time step was about 0.01 ms. In most cases, no more than three iterations were needed for the convergence. When the above global iteration process is employed, and the time step Δt is sufficiently small (say, of the order of 10^{-2} ms), the internal iteration loop (steps 5 and 6) becomes unnecessary. Note that reasonable accuracy can be obtained with only 20 grid intervals inside the droplet. In such a case, the total CPU time required for a single droplet analysis is about 5 s on a VAX-780.

The energy equation (33) for the extended model is solved by the fully implicit iterative finite difference method. The space derivatives are approximated by central differences and the finite-difference grid spacings $(\Delta\eta, \Delta\theta)$ are uniform. The difficulties associated with integral boundary condition (36) can be overcome by taking advantage of the linearity of the problem. Assume that the temperature distribution inside the droplet is known at some time level τ: $Z = Z_\tau$. Then, the temperature at the new time level $(\tau+\Delta\tau)$ is represented as a linear combination of two functions

$$Z = Z_1(\eta, \theta, \tau) + AZ_2(\eta, \theta, \tau) \tag{40}$$

where Z_1 and Z_2 are the partial solutions of equation (33). Both functions Z_1 and Z_2 satisfy the symmetry conditions (37). At time τ, the values of functions Z_1 and Z_2 are prescribed as

$$Z_1(\eta, \theta, \tau) = Z(\eta, \theta, \tau) \tag{41}$$

$$Z_2(\eta, \theta, \tau) = 0. \tag{42}$$

The surface values of functions Z_1 and Z_2 at time $(\tau+\Delta\tau)$ are given as

$$Z_1(1, \theta, \tau+\Delta\tau) = Z_1(1, \theta, \tau) \tag{43}$$

$$Z_2(1, \theta, \tau+\Delta\tau) = 1. \tag{44}$$

It is easily seen that the solutions $Z_1(\eta, \theta, \tau+\Delta\tau)$ and $Z_2(\eta, \theta, \tau+\Delta\tau)$ at the new time level $(\tau+\Delta\tau)$ can be found independently of one another. Then, the constant A in equation (40) is determined using boundary condition (36). Note that A will vary with time.

The number of mesh intervals within the droplet was 70×60 in the radial and angular directions, respectively. The time step was about 10^{-3} ms. The mesh independence of computations has been confirmed using the more dense mesh 100×70. The total CPU time for a typical run is 5–6 h on a VAX-780.

RESULTS AND DISCUSSION

The applicability of the simplified models should be checked by comparison with more advanced numerical solutions. Unfortunately, such a verification is still possible only for the stagnant droplet case ($Re = 0$). We compared the simplified gas-phase model with the steady-state calculations by Kent [41] for n-heptane and the transient analysis by Hubbard *et al.* [19] for n-octane. In both of these studies, the spatial variation of gas properties has been taken into account. The detailed discussion of this comparison is presented in the previous publication [18]. The vaporization rate of a droplet is extremely sensitive to the method used for the evaluation of physical properties. A very good agreement with the exact variable properties calculations is achieved by applying the '1/3 rule' for averaging of the gas mixture properties.

The following results refer to the standard cases of n-decane droplets of initial radius $r_0 = 50$ μm and temperature $T_0 = 300$ K which are injected into an air stream at $T_\infty = 1500$ K, $P_\infty = 10$ atm. The physical properties used in the computations are given in the Appendix. In Figs. 2 and 3, the dynamic and vaporization history of the droplet is illustrated for the case when the droplet with the initial velocity $U = 15$ m s^{-1} is inserted into a quiescent air environment. The initial Reynolds number for the gas phase is 105. The calculations were made using the extended liquid heating model with the internal circulation. In some figures, the comparison is made with the simplified models of liquid heating, and there curve 1 denotes the extended model while curves 2 and 3 refer to the 'infinite conductivity' and 'conduction limit' models, respectively. Curve 4 represents the 'effective conductivity' model with the factor χ calculated as a function of the liquid Peclet number using equation (39). Figures 2(a)–(c) show the temporary variation of the non-dimensional droplet radius, (r_s/r_0), surface temperature, T_s, and the instantaneous vaporization rate, $(\dot{m}/m_0)$, respectively. Here, m_0 is the initial droplet mass. The results for the extended liquid heating model fall, in general, between those for the 'infinite conductivity' and 'conduction limit' model. Interestingly, the curves of the 'effective diffusivity' model almost coincide with those of the extended model.

Figure 2(d) shows the history of the average Lewis number $\bar{L}e = \bar{k}_g/(\bar{\rho}_g \bar{D}_g \bar{C}_{pg})$, and the parameter ϕ (see equation (22)) in the gas film. Initially, when the droplet surface is cold and the vapor concentration in the film is low, the Lewis number is very high because the diffusion coefficient of heavy hydrocarbon vapor in air is much lower than the thermal diffusivity of air. As fuel concentration in the gas film grows, the Lewis number decreases, remaining, however, larger than 1. The parameter ϕ varies from 1.05 to 1.2 in the course of vaporization. However, even its small deviation from 1.0 (value assumed by the classical theory) results in the considerable difference between the values of B_M and B_T (Fig. 2(e)).

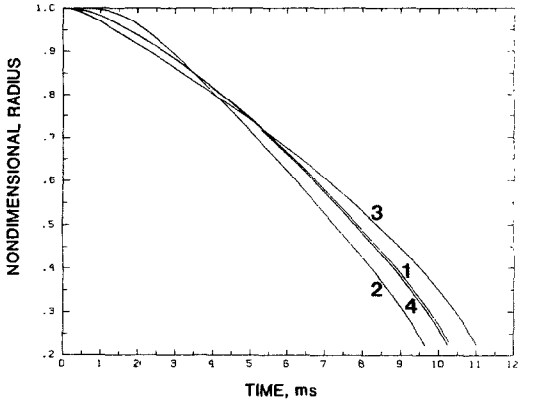

FIG. 2(a). Non-dimensional droplet radius vs time: extended model (curve 1), infinite conductivity model (curve 2), conduction limit model (curve 3), and effective conductivity model (curve 4).

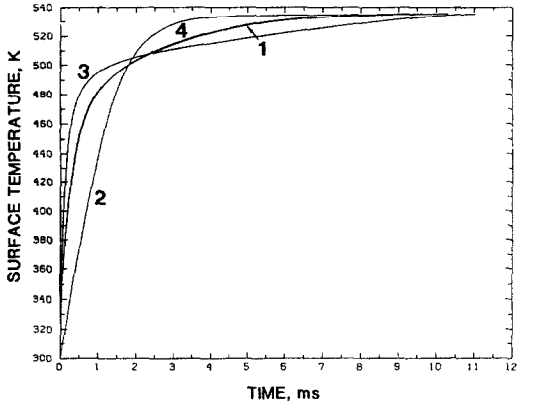

FIG. 2(b). Surface temperature (K) vs time: various models.

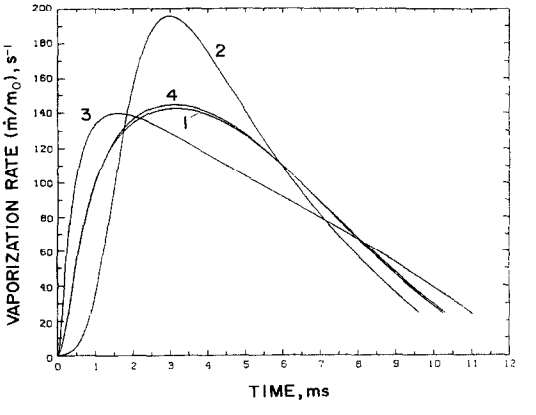

FIG. 2(c). Vaporization rate vs time: various models.

Figure 2(f) illustrates the time variations of the gas phase and liquid phase Reynolds numbers. Gas phase Reynolds number, Re, decreases monotonically as the droplet decelerates and its diameter diminishes. During the first half of the droplet life, the Reynolds number for the liquid interior appears to be considerably higher than Re for the gas. This fact was first predicted in refs. [25, 26] based on the scale analy-

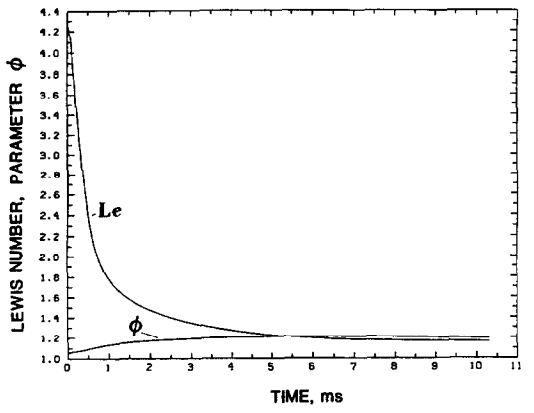

FIG. 2(d). Lewis number vs time and parameter ϕ vs time.

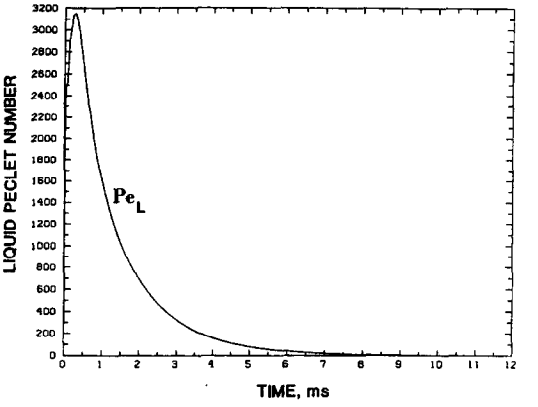

FIG. 2(g). Liquid Peclet number vs time.

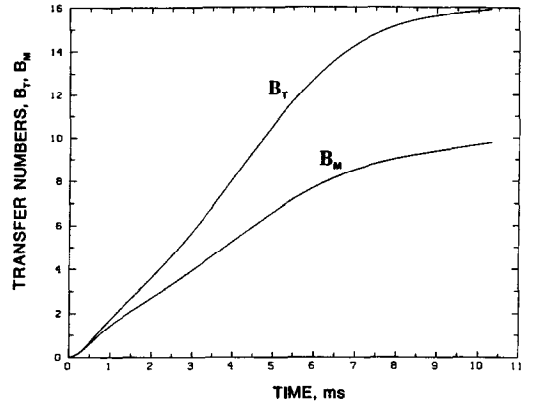

FIG. 2(e). Transfer numbers vs time.

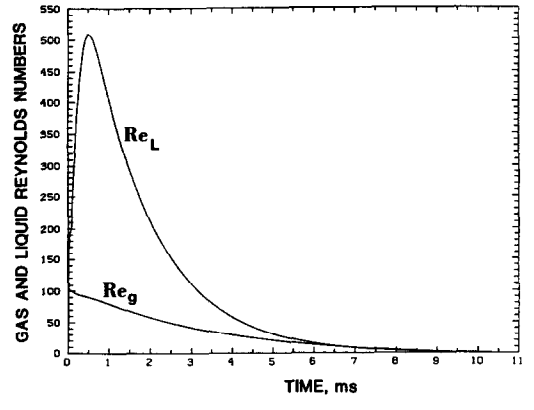

FIG. 2(f). Gas and liquid Reynolds numbers vs time.

sis. The maximum on the curve $Re_L = Re_L(t)$ at small times is related to the variation of the liquid dynamic viscosity (see equation (30)), which was evaluated at the surface temperature.

The liquid Peclet number behavior is qualitatively similar to that of Re_L (Fig. 2(g)). During the considerable part of the droplet vaporization period, the Peclet number inside the droplet remains very high ($Pe_L \gg 1$) indicating that the heat transfer within the droplet should be of the convection-dominated type.

Figure 3 illustrates the isotherms inside the droplet at different times. Here, gas flows toward the right relative to the droplet center. The isotherms are plotted for the temperature levels: $T_i = T_{min} + (T_{max} - T_{min})i/10$ where $(i = 1, 2, \ldots, 10)$, and T_{min} and T_{max} represent the minimum and maximum temperature inside the droplet at a given time. The values of T_{min} and T_{max} are also shown.

At very short times $t < 0.025$ ms, the heat is transferred from the surface primarily by thermal conduction. At $t = 0.05$ ms, the convective effects become very important and cause the distortion of the spheri-

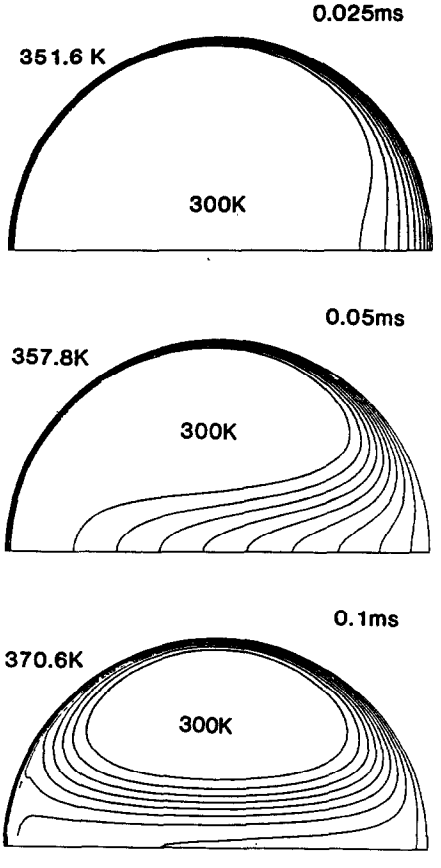

FIG. 3(a). Liquid isotherms: 0.025, 0.05, and 0.1 s.

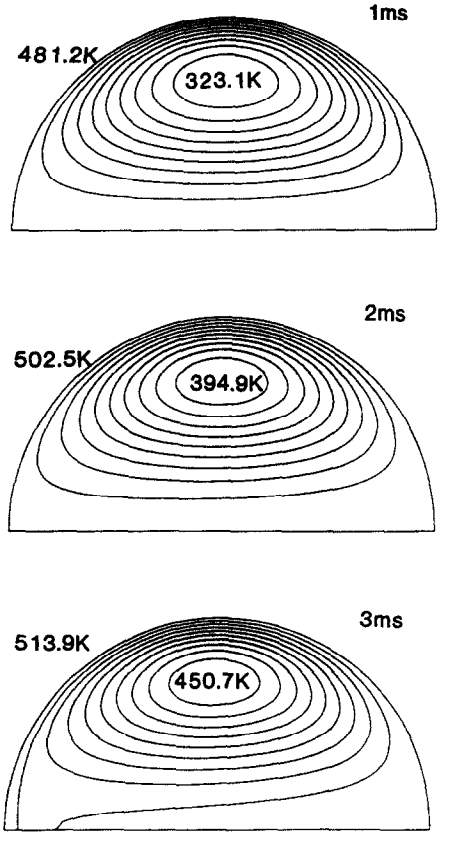

FIG. 3(b). Liquid isotherms: 1, 2, and 3 ms.

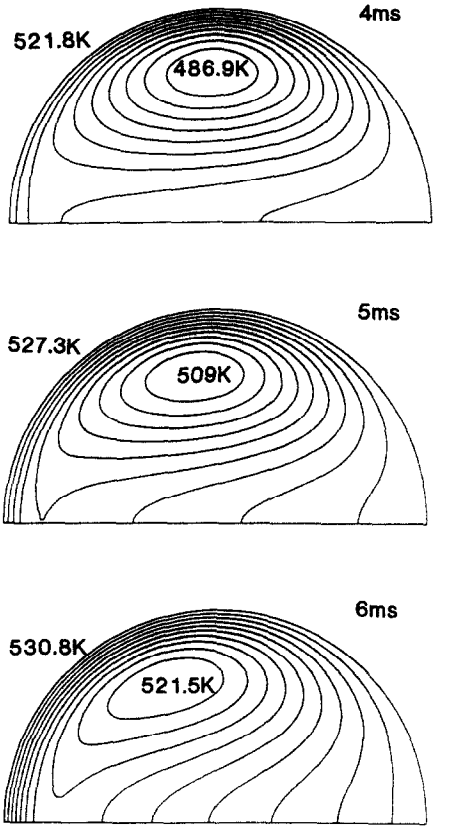

FIG. 3(c). Liquid isotherms: 4, 5, and 6 ms.

cal symmetry of the temperature field inside the droplet. During the time interval $t = 0.1$–4.0, the isotherm patterns within the droplet are very similar to those of the streamlines. This fact provides the qualitative confirmation of the 'vortex model' at high Pe_L. However, as liquid phase Peclet number, Pe_L, decreases below 100 ($t = 5$ ms), the reverse transition from convection- to conduction-dominated heat transfer is observed.

The mechanism of the internal heat transfer may change considerably in the course of the droplet vaporization. In the above example, during the first 30–40% of the droplet lifetime, when the liquid Peclet number exceeds ~ 100, the heat is transferred in accordance with the prediction of the 'vortex model'. During the last third of the droplet life, when $Pe_L \leqslant 10$, the heat transfer mechanism is more similar to that of the 'conduction limit model'. A smooth transition between these two regimes occurs in the range $100 \geqslant Pe_L \geqslant 10$. From the computational point of view, it may be suggested that the switch between the 'vortex' and 'conduction limit' models should be made at some 'critical' liquid Peclet number, say $Pe_L = 20$. However, the more convenient approach seems to use the 'effective conductivity model' with the χ-factor given by equation (39).

It should be recognized that the 'effective conductivity model' does not detail the important physical features of the problem associated with the internal circulation. However, this model reflects properly the global effect of the internal liquid motion and mixing on heat transfer within droplets. The important advantage of the 'effective conductivity model' is that the same computational scheme may be applied for all droplet groups in the spray in the wide range of Reynolds and Peclet numbers.

In order to test the 'effective conductivity model' in more complicated situations, we considered the thermal and vaporization history of a droplet in a fluctuating flow field. Such a problem is very relevant to the analysis of combustion instability in liquid-fueled ramjets or liquid propellant rockets where the pressure, velocity and gas flow temperature may oscillate in the frequency range of 100–15 000 Hz [42]. In the following example, we consider a simple case in which the gas flow velocity varies as a prescribed harmonic function of time

$$U_\infty = \bar{U}_\infty + A_u \cos 2\pi f t. \tag{45}$$

This might occur at a pressure node of the oscillation, for example. We assume, however, that the pressure and temperature of the gas remain constant. The velocity amplitude is set as $A_u = 15\ \mathrm{m\ s^{-1}}$, the frequency is $f = 500$ Hz, and the initial droplet velocity is equal to the average gas velocity $U_0 = \bar{U}_\infty$. All other par-

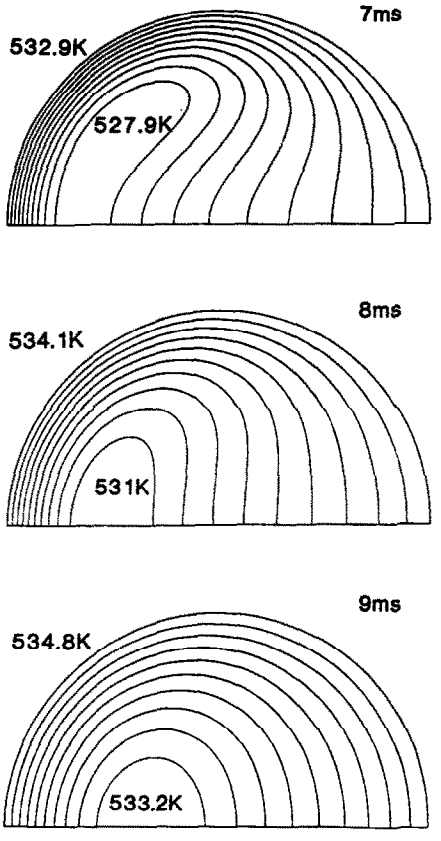

FIG. 3(d). Liquid isotherms: 7, 8, and 9 ms.

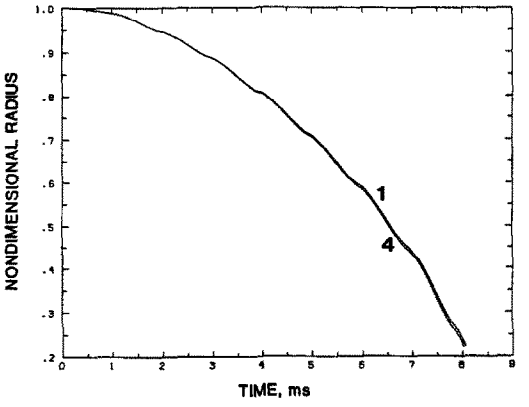

FIG. 4(b). Non-dimensional droplet radius vs time.

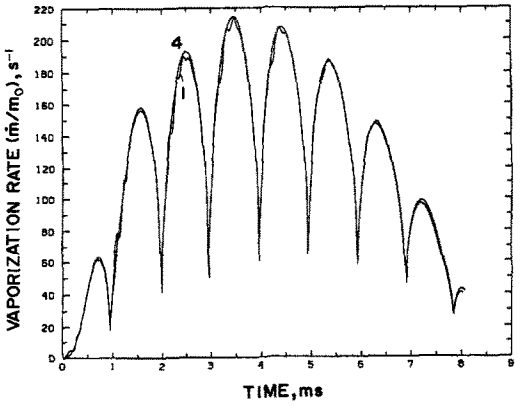

FIG. 4(c). Vaporization rate vs time.

ameters are selected to be the same as in the previous example.

The results of the calculations are shown in Figs. 4(a)–(c). Figure 4(a) shows the gas flow and droplet velocities as functions of time. Figures 4(b) and (c) show the instantaneous droplet radius and vaporization rate, respectively. Curves 1 and 4 refer to the extended model of liquid heating and to the 'effective conductivity model', respectively. The vaporization rate is considerably affected by the gas velocity oscillations. The sharp minima in Fig. 4(c) correspond to times when the relative gas-to-droplet velocity become zero (interception points at Fig. 4(a)). Again, the simplified 'effective conductivity model' agrees very well with the extended model of internal liquid heating. Certain details in the behavior are, however, not captured by the effective diffusivity model.

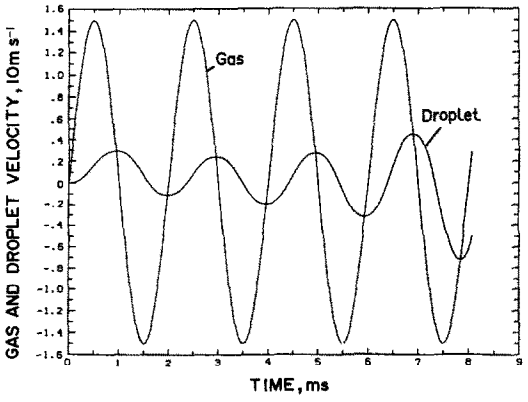

FIG. 4(a). Gas and droplet velocities vs time.

The above results indicate that the 'effective conductivity' approach may be recommended for use in the droplet vaporization model. The advantages of this new vaporization model are its simplicity, applicability to the wide range of parameters (Re, B, etc.), and a low amount of computer time required per single droplet life calculation. The proposed model agrees very well with the existing exact numerical solutions at $Re = 0$, and reasonably predicts the droplet vaporization rate at high Reynolds numbers. The model uses the available state-of-the-art semi-empirical correlations for the total droplet drag coefficient, C_D, friction drag coefficient, C_F, Nusselt and Sherwood numbers, Nu_0 and Sh_0, as well as the theoretically-predicted relationships for the relative changes of the film thickness, $F_T(B_T)$ and $F_M(B_M)$, and for the effective conductivity factor, $\chi(Pe_L)$. Some of these correlations, however, have been established for the limited range of the working parameters (Re, B_T, B_M) or for the different geometrical configurations (wedge, stagnation point, etc.). Therefore, the extension and improvement of the above correlations are

desirable. The further refinements of the present simplified model can be made by comparison with the advanced numerical models when they become available.

CONCLUSION

A new approximate model of vaporization of a moving fuel droplet has been formulated. This model represents the extension of the classical droplet vaporization model and includes such important effects as variable physical properties and non-unitary Lewis number in the gas phase, influence of the Stefan flow (blowing) on heat and mass transfer, and the effect of the transient liquid heating inside the internally circulating droplet. The gas phase calculations are based on the one-dimensional 'stagnant film theory' which has been extended to incorporate the Stefan flow effect on the thicknesses of the thermal and diffusional films. The transient liquid heating inside the droplet is calculated using the spherically symmetric 'effective conductivity model'. The 'effective' thermal conductivity of the liquid fuel, k_{eff}, is introduced to account for the heat enhancement due to the internal liquid circulation. The factor $\chi = k_{\text{eff}}/k_{\text{L}}$ depends on the instantaneous Peclet number in the liquid phase. The relationship $\chi = \chi(Pe_{\text{L}})$ has been found from the Johns and Beckmann study [38] on mass transfer within circulating droplets. The results of calculations with the 'effective conductivity model' appear to be in a very good agreement with those predicted by the extended liquid heating model that includes the solution of the two-dimensional equation of convective heat transfer within a circulating vaporizing droplet.

The proposed model may be used in the wide range of droplet sizes and Reynolds numbers. It requires a relatively small amount of computational time per single droplet life history. Therefore, this model is suitable for the spray combustion calculations which simultaneously trace the life histories of many individual droplets.

Acknowledgement—This research has been sponsored by the Office of Naval Research.

REFERENCES

1. W. A. Sirignano, Fuel droplet vaporization and spray combustion theory, *Prog. Energy Combust. Sci.* **9,** 291–332 (1983).
2. W. A. Sirignano, An integrated approach to spray combustion model development, *Combust. Sci. Technol.* **58,** 231–251 (1988). Also see ASME 107th WAM, Anaheim, California (December 1986).
3. W. A. Sirignano, The formulation of spray combustion models: resolution compared to droplet spacing, *J. Heat Transfer* **108**(3), 633 (1986).
4. W. A. Sirignano, Spray combustion simulation. In *Numerical Simulation of Combustion Phenomena* (Edited by R. Glowinski, B. Larrouturou and R. Teman). Springer, Heidelberg (1985).
5. G. M. Faeth, Current status of droplet and liquid combustion, *Prog. Energy Combust. Sci.* **3,** 191–224 (1977).
6. C. K. Law, Recent advances in droplet vaporization and combustion, *Prog. Energy Combust. Sci.* **8,** 171–201 (1982).
7. A. Williams, *Combustion of Sprays of Liquid Fuels*. Elek Science, London (1976).
8. K. K. Kuo, *Principles of Combustion*. Wiley, New York (1986).
9. F. A. Williams, *Combustion Theory*. Benjamin/Cummings, Menlo Park, California (1985).
10. C. K. Law and W. A. Sirignano, Unsteady droplet combustion with droplet heating—II: conduction limit, *Combust. Flame* **28,** 175–186 (1977).
11. M. Renksizbulut and M. C. Yuen, Numerical study of droplet evaporation in a high-temperature stream, *J. Heat Transfer* **105,** 389–397 (1983).
12. G. Patnaik, W. A. Sirignano, H. A. Dwyer and B. R. Sanders, A numerical technique for the solution of a vaporizing fuel droplet. Dynamics of reaction systems, *Prog. Astronaut. Aeronaut.* **105,** 253–266 (1986).
13. H. A. Dwyer and B. R. Sanders, Detailed computation of unsteady droplet dynamics, *Twentieth Symp. (Int.) on Combustion*, The Combustion Institute, pp. 1743–1749 (1984).
14. B. R. Sanders and H. A. Dwyer, Modeling unsteady droplet combustion processes. *Proc. 2nd ASME/JSME Thermal Engng Joint Conf.*, Honolulu, Vol. 1, pp. 3–10 (March 1987).
15. R. Haywood and M. Renksizbulut, On variable property, blowing and transient effects in convective droplet evaporation with internal circulation, *Proc. Eighth Int. Heat Transfer Conf.*, San Francisco, Vol. 4, pp. 1861–1866 (August 1986).
16. M. Renksizbulut and R. J. Haywood, Transient droplet evaporation with variable properties and internal circulation at intermediate Reynolds numbers, *Int. J. Multiphase Flow* **14,** 189–202 (1988).
17. M. C. Yuen and L. W. Chen, On drag of evaporating liquid droplets, *Combust. Sci. Technol.* **14,** 147–154 (1976).
18. B. Abramzon and W. A. Sirignano, Approximate theory of a single droplet vaporization in a convective field: effects of variable properties, Stefan flow and transient liquid heating, *Proc. 2nd ASME–JSME Thermal Engng Joint Conf.*, Honolulu, Hawaii, Vol. 1, pp. 11–18 (March 1987).
19. G. L. Hubbard, V. E. Denny and A. F. Mills, Droplet vaporization: effects of transients and variable properties, *Int. J. Heat Mass Transfer* **18,** 1003–1008 (1975).
20. R. B. Bird, W. E. Stewart and E. N. Lightfoot, *Transport Phenomena*. Wiley, New York (1960).
21. D. A. Frank-Kamenetskii, *Diffusion and Heat Transfer in Chemical Kinetics* (2nd Edn). Plenum Press, New York (1969).
22. H. Schlichting, *Boundary-layer Theory* (7th Edn). McGraw-Hill, New York (1979).
23. M. Renksizbulut and M. C. Yuen, Experimental study of droplet evaporation in high-temperature air stream, *J. Heat Transfer* **105,** 384–388 (1983).
24. R. Clift, J. R. Grace and M. E. Weber, *Bubbles, Drops and Particles*. Academic Press, New York (1978).
25. S. Prakash and W. A. Sirignano, Liquid fuel droplet heating with internal circulation, *Int. J. Heat Mass Transfer* **21,** 885–895 (1978).
26. S. Prakash and W. A. Sirignano, Theory of convective droplet vaporization with unsteady heat transfer in the circulating liquid phase, *Int. J. Heat Mass Transfer* **23,** 253–268 (1980).
27. A. Y. Tong and W. A. Sirignano, Analysis of vaporizing droplet with slip, internal circulation, and unsteady liquid-phase and quasi-steady gas-phase heat transfer, *ASME/JSME Thermal Engng Joint Conf. Proc.*, Vol. 2, pp. 481–487 (1983).
28. A. Y. Tong and W. A. Sirignano, Multicomponent drop-

let vaporization in a high temperature gas, *Combust. Flame* **66**, 221–235 (1986).
29. A. Y. Tong and W. A. Sirignano, Multicomponent transient droplet vaporization: integral equation formulation and approximate solution, *Numer. Heat Transfer* **10**, 253–278 (1986).
30. S. K. Aggarwal, A. Y. Tong and W. A. Sirignano, A comparison of vaporization models in spray calculations, *AIAA J.* **22**(10), 1448–1457 (1984).
31. D. G. Talley and S. C. Yao, A semi-empirical approach to thermal and composition transients inside vaporizing fuel droplets, *Twenty-first Symp. (Int.) on Combustion*, The Combustion Institute, pp. 609–616 (1986).
32. J. D. Jin and G. L. Borman, A model for multicomponent droplet vaporization at high ambient pressures, *Combustion Emission and Analysis*, P-162, pp. 213–223. SAE, Inc. (1985).
33. R. Kronig and J. C. Brink, On the theory of extraction from falling droplets, *Appl. Scient. Res.* **A2**, 142–154 (1951).
34. V. Ya. Rivkind and G. M. Ryskin, Flow structure in motion of a spherical drop in a fluid medium at intermediate Reynolds numbers, *Fluid Dyn.* **1**, 5–12 (1976).
35. D. L. R. Oliver and J. N. Chung, Flow about a fluid sphere at low to moderate Reynolds numbers, *J. Fluid Mech.* **177**, 1–18 (1987).
36. B. P. LeClair, A. E. Hamielec, H. R. Pruppacher and W. D. Hall, A theoretical and experimental study of the internal circulation in water drops falling at terminal velocity in air, *J. Atmos. Sci.* **29**(4), 728–740 (1972).
37. H. W. Emmons, The film combustion of liquid fuel, *Z. Angew. Math. Mech. (ZAMM)* **36**, 60 (1956).
38. L. E. Johns and R. B. Beckmann, Mechanism of dispersed-phase mass transfer in viscous, single-drop extraction system, *A.I.Ch.E. Jl* **12**(1), 10–16 (1966).
39. D. Porter, *Computational Physics*. Wiley, New York (1973).
40. D. K. Edwards, V. E. Denny and A. F. Mills, *Transfer Processes: an Introduction to Diffusion, Convection and Radiation* (2nd Edn). McGraw-Hill, New York (1979).
41. J. C. Kent, Quasi-steady diffusion-controlled droplet evaporation and condensation, *Appl. Scient. Res.* **28**, 315–345 (1973).
42. D. T. Harrje and F. H. Reardon (Editors), *Liquid Propellant Rocket Combustion Instability*, Scientific and Technical Information Office, NASA, SP-194, Washington (1972).
43. L. Crocco, Theoretical studies on liquid propellant rocket instability, *Tenth Symp. (Int.) on Combustion*, The Combustion Institute, p. 1118 (1965).

APPENDIX. PHYSICAL PROPERTIES

Physical properties of vapor/air mixture were calculated at reference film conditions (equations (4)) using the standard additive rules for an ideal gas

$$\bar{\rho}_g = [(\bar{Y}_F/\rho_F)+(1-\bar{Y}_F)/\rho_{air}]^{-1}$$

$$\bar{C}_{pg} = C_{pF}\bar{Y}_F + C_{pair}(1-Y_F).$$

The Wilke rule was used for the dynamic viscosity and thermal conductivity [40]. Fuel properties were extracted from the various sources and approximated as a function of the temperature [18]. Thus, for n-decane, the following correlations were used:

saturated vapor pressure:

$$P_{Fs} = \exp[11.495-5141.36/T_s]\ \text{[atm]}$$

latent heat of vaporization:

$$L(T_s) = 9.453(619.0-T_s)^{0.38}\ [\text{kcal kg}^{-1}]$$

binary diffusion coefficient:

$$D = 5.46\times10^{-6}\,(T/300)^{1.583}\,P^{-1}\ [\text{m}^2\,\text{s}^{-1}]$$

vapor thermal conductivity:

$$k_F = 2.9\times10^{-6}\,(T/300)^{1.8}\ [\text{kcal m}^{-1}\,\text{s}^{-1}\,\text{K}^{-1}]$$

vapor dynamic viscosity:

$$\mu_F = [0.564+1.75\times10^{-3}(T-300)]\times10^{-5}\ [\text{kg m}^{-1}\,\text{s}^{-1}]$$

vapor specific heat:

$$C_{pF} = 0.02547+1.377T_1-0.4T_1^2+0.113T_1^3 \text{ at } T_1 < 0.8$$

and

$$C_{pF} = 0.0982+1.304T_1-0.593T_1^2+0.101T_1^3 \text{ at } T_1 > 0.8.$$

Here $T_1 = T/1000$ K and C_p is expressed in kcal kg^{-1} K^{-1}.

Liquid fuel properties (except viscosity) were assumed to be constant and evaluated at some average temperature $\bar{T}_L = 0.5\,(T_0+T_{boil})$ where T_{boil} is the boiling temperature at a given pressure. Thus, for example, at $\bar{T}_L = 400$ K

$$\rho_L = 6.42\times10^{-4}\ \text{kg m}^{-3};$$

$$C_{pL} = 0.602\ \text{kcal kg}^{-1}\,\text{K}^{-1};$$

$$k_L = 2.52\times10^{-5}\ \text{kcal m}^{-1}\,\text{K}^{-1}.$$

The liquid dynamic viscosity which appears in equation (30) was calculated at the surface temperature using the following approximation:

$$\mu = 9.0\times10^{-4}\exp(T_s/300-1)\ \text{kg m}^{-1}\,\text{s}^{-1}.$$

MODELE DE VAPORISATION DE GOUTTELETTE POUR LES CALCULS DE LA COMBUSTION

Résumé—On réexamine le modèle classique de la vaporisation de gouttelettes pour développer l'algorithme de calcul simple mais suffisamment préçis qui peut être utilisé dans les calculs de combustion de liquide pulvérisé. Le nouveau modèle inclut les effets des propriétés thermophysiques variables, d'un nombre de Lewis différent de l'unité dans le film gazeux, de l'effet de l'écoulement de Stefan sur le transfert de chaleur et de masse entre la gouttelette et le gaz et celui de la circulation interne et du chauffage variable du liquide. Pour évaluer les modèles simplifés concurrents du chauffage de la goutte, on considère le transfert de chaleur dans une goutte avec circulation; une "conductivité effective" monodimensionnelle est alors formulée. Pour illustration, on analyse l'histoire dynamique de la vaporisation des gouttelettes injectées dans des courants d'air au repos ou fluctuants.

EIN TROPFENVERDAMPFUNGSMODELL FÜR DIE BERECHNUNG DER VERBRENNUNG VON BRENNSTOFFNEBEL

Zusammenfassung—Das klassische Tropfenverdampfungsmodell wird angepaßt, um einen einfachen, aber hinreichend genauen Algorithmus für die Berechnung der Verbrennung von Brennstoffnebel zu entwickeln. Das neue Modell berücksichtigt folgende Effekte: die Auswirkungen veränderlicher thermophysikalischer Stoffeigenschaften, die Abweichung der Lewis-Zahl für den Gasfilm vom Wert "eins", die Auswirkung des Stefan–Stroms auf den Wärme- und Stoffübergang zwischen Tropfen und Gas, die Einflüsse einer internen Zirkulationsströmung und einer Aufheizung der Flüssigkeit. Um die in Konkurrenz befindlichen vereinfachten Modelle für die Tropfenaufheizung einschätzen zu können, wurde ein verbessertes und erweitertes Modell der Wärmeübertragung in einem sich bewegenden und zirkulierenden Tropfen betrachtet. Ein vereinfachtes eindimensionales Modell für die "effektive Leitfähigkeit" wird für den Fall der instationären Aufheizung der Flüssigkeit mit interner Zirkulationsströmung formuliert. Zur Illustration werden die Bewegungs- und Verdampfungsverläufe von Tropfen analysiert, die in einen stetigen und fluktuierenden Heißluftstrom eingespritzt werden.

ИСПОЛЬЗОВАНИЕ МОДЕЛИ КАПЕЛЬНОГО ИСПАРЕНИЯ ДЛЯ РАСЧЕТА ГОРЕНИЯ РАСПЫЛА

Аннотация—Пересмотрена классическая модель испарения капель для разработки простого, но достаточно точного расчетного алгоритма, который может использоваться для расчета процесса горения распыла. Новая модель учитывает различие теплофизических свойств, отличие числа Льюиса от единицы в газовой пленке, влияние потока Стефана на тепло-и массоперенос между каплей и газом и влияние внутренней циркуляции и нестационарного нагрева жидкости. Для оценки аналогичных упрощенных моделей нагрева капель рассмотрена более совершенная модель теплопереноса внутри движущейся циркулирующей капли. Сформулирована упрощенная одномерная модель "эффективной проводимости", описывающая нестационарный процесс нагрева жидкости с внутренней циркуляцией. В качестве иллюстрации проанализированы динамика и процесс испарения капель, вдуваемых в стационарный и пульсирующий потоки горячего воздуха.